Rearrangement of interstitial defects in alpha-Fe under extreme condition

Alain Chartier, Mihai Cosmin Marinica

Rearrangement of interstitial defects in alpha-Fe under extreme condition

A. Chartier
CEA, DEN, Service de Corrosion et du Comportement des Matériaux dans leur Environnement (SCCME), Université Paris-Saclay, F-91191 Gif-sur-Yvette, France

M.-C. Marinica
CEA, DEN, Service de Recherches de Métallurgie Physique (SRMP), Université Paris-Saclay, F-91191 Gif-sur-Yvette, France

(Received …)

In this study, by theoretical means, we reveal the main mechanisms that underpin the microstructure evolution driven by the formation of self-interstitial atoms (SIAs) clusters in body centered cubic iron under extreme conditions. Using Frenkel pairs accumulation simulations we point the complex interplay between the two families of interstitial defects, the dislocation loops with Burgers vectors <100> and ½<111> and the tridimensional C15 clusters. We reconcile the previous sparse understanding of microstructure evolution that put in opposition various mechanisms of defects formation by showing that both ½ <111> loops self-interactions and C15 clusters transformations produce <100> loops. Moreover, we exhibit the fact that these tri-dimensional clusters can form under irradiations with only the Frenkel pair accumulation that mimics electron irradiation and not only in high-energy cascades as it was previously stated. Finally, we show that the tridimensional C15 clusters even precede production of loops under irradiation.

DOI:

I Introduction: 2D and 3D defects in irradiated bcc-iron

The performance of materials under extreme conditions is driven by the formation and the mobility of clusters of vacancies and interstitial atoms. Vacancies and self-interstitial atoms (SIAs) form either two or three-dimensional clusters depending on their sizes and mainly because of the competition between the interface and the bulk energies. In body centered cubic (bcc) metals, the clusters of vacancy behave similarly [1], while the SIAs clusters underlay complex energetic landscape with plenteous morphologies [2, 3, 4, 5], iron being one of the more exotic [6, 7].
In bcc transition metals, single SIA generally forms a crowdion that is a defect aligned along the <111> direction [8, 9, 10, 11, 12]. Few of these dumbbells can pack together into bundles, forming small dislocation loops. In iron, resistivity recovery as well as internal friction experiments and DFT computations show that the most stable configuration for single SIA is a <110> dumbbell. Packed dumbbells keep this orientation until around five SIAs and then change orientation above, into <111> direction according to DFT predictions [2, 13, 14].
Dumbbells in iron may also transform into three-dimensional structures with symmetry corresponding to C15 Laves phase [6, 14, 15]. These C15 structures are stable, immobile and exhibit large antiferromagnetic moments. However, for higher number of SIAs, they face competition with nanometric-sized dislocation loops. According to a recent DFT informed discrete-continuum model [6], C15 clusters may transform into ½ <111> loops for more than around 50 SIAs, or into <100> loops for more than around 90 SIAs.

Indeed, transmission electron microscopy (TEM) observations in bcc transition metals reveal the existence of planar loops. They can have the Burgers vector aligned along either ½<111> (highly mobile) or <100> (immobile), depending on temperature [16, 17, 18, 19, 12]. Dislocation loops with ½<111> Burgers vector are dominant in most bcc metals, and are therefore presumed to be the most stable configurations for bundling crowdions. In iron, magnetism controls the relative stability of both morphologies. The ½<111> loops are the most stable at low temperature while above 800K it is the <100> loops [10]. These <100> loops are also observed in irradiated iron at low temperature. However, though numerous studies tackle their formation, as we will see below, the very details of the mechanisms at work are still subject of intense researches.
Masters [16] investigated first experimentally the formation of <100> loops in irradiated iron in the absence of vacancy cluster. He suggested that the formation of these loops is based on the interaction between two ½<111> loops. Eyre and Bullough [18] rather suggested that ½<110> loops are involved in the formation of <100> dislocation loops. Decades later, based on the seminal work of Osetsky *et al* [20] on the ½<111> loops interaction, Marian *et al* [21] explored the two possibilities by means of atomistic simulations. They showed that the formation of <100> segments may happen from the interaction between two ½<111> loops with appropriate sizes and specific orientations. They concluded that <100> loops can be formed from ½<111> loops. Xu *et al* [22] showed the complete transformation of two colliding ½<111> loops into <100> loop. This process is stochastic in nature according to Xu *et al* [22], and highly infrequent due to the strict conditions required. However, using TEM, Arakawa *et al* [23] did not put in evidence any <100> loops while examining tens of ½<111> loops reactions. Recently, Wang *et al* [24] added another path for the formation of <100> loops, based on a ternary loops reaction which involves also ½<111> loops. In addition, Chen *et al* [25] pointed

in their study that <100> loops may result from the re-arrangement and reorientation of a single crowdion cluster.
Besides, other authors returned to the role of single events like thermal spikes or displacement cascades for the creation of <100> loops in iron. Thus, recent simulations by Khara *et al* [26] showed that both ½ <111> loops and <100> loops may emerge from one single track induced by swift heavy ion. Further, Peng *et al* [27] reminded that displacement cascades produce shockwaves around them. In iron, they promote the transformation of SIAs into <100> loops by a so-called punch out mechanism, at distance from the cascade cores. These loops also arise directly inside cascades according to Calder *et al* [28], with an increasing probability of formation with pka mass. Granberg *et al* [29] provided incremental insights on this point and evidenced that overlap of cascades on pre-existing primary radiation damage readily produces <100> loops too.
Alternatively, Zhang *et al* [30] called for the nucleation of very stable C15 clusters. This class of clusters, identified as "sessile" and "metastable" clusters in Gao *et al* [31] or later as C15 clusters in Marinica *et al* [14] – appear directly inside high-energy cascades as observed too by Zarkadoula *et al* [32] or in overlapping cascades after Byggmästar *et al* [33]. Zhang *et al* [30] argued that once formed, C15 clusters grow by trapping small mobile interstitials induced by irradiation. C15 clusters subsequently transform into ½<111> loops or <100> loops at equivalent amount. While this scenario is based on empirical potential simulations, *ab initio* calculations performed later by Alexander *et al* [6] bring thorough support. One may also anticipate that <100> loops might form with a much lower probability since they require the stabilization and transformation of much bigger C15 clusters – by roughly forty SIAs – than ½<111> loops [6].

Using extensively molecular dynamics (MD) simulations in iron, we investigate the nucleation and growth of interstitials defects, such as C15 clusters and both ½<111> and <100> loops by irradiation. We apply a demarche introduced first by Limoge *et al* [34] in which periodic creation of Frenkel pairs is designed to mimic irradiation. Such methodology already provided valuable insights on mechanisms of irradiation induced amorphization in metallic systems, like copper-titanium intermetallics [35] or Ni-Zr solid solution [36, 37], as well as in oxides [38, 39] or in graphite [40].
With this methodology, in nano-metric supercells, we scrutinize on the fly the evolution of defects – including C15 clusters and both ½<111> loops and <100> loops – as a function of dose up to 1.0 dpa. In addition to these integrated simulations, we rationalize our observations by applying dedicated calculations involving single C15 cluster. In this regard, we introduce SIAs only (without the counter-defect, vacancy) close to C15 clusters of different sizes, in a similar manner as performed recently by Monasterio *et al* [41] and taking advantage of previous estimations [6].
Combination of both types of simulations allows us to provide a new route for the nucleation of <100> loops along with insights on formation and stability of C15 clusters as explained below.

II Methodology: Frenkel pairs accumulation

We perform all our molecular dynamics simulations using the LAMMPS code [42] with the M07 EAM potential for iron [14, 43]. This potential has the particularity of satisfactory reproducing relative formation energies of small loops with respect to C15 clusters, in agreement with 0 K *ab initio* calculations [6, 14]. We design two sets of simulations: the first set explores the entire process of nucleation and growth of defect clusters and/or loops by irradiation while the second one targets the transformation of specific configurations of C15 clusters.

In the first set of simulations, irradiation is mimicked by performing Frenkel pair accumulation (FPA) in a chosen supercell, following previous studies [34, 35, 38, 39]. Herein, iron atoms are randomly chosen in the entire supercell and randomly displaced at a distance of more than 1.2 Å than any other atom. The time between each of these displacements is set to 2 ps. Interstitials and vacancies created lead to the increase of pressure and of temperature. Both are driven back to their target values (300K and 0 GPa) within 2 ps thanks to careful controls relying on Berendsen thermostat and barostat.
In order to track finite size effects, we investigate two supercell sizes, one containing 11664000 atoms (called hereafter big supercell) of volume 51.5 × 51.5 × 51.5 nm^3 and the other one containing 1458000 atoms (called hereafter small supercell) of volume 25.7 × 25.7 × 25.7 nm^3. 2500 and 400 Frenkel pairs were introduced in the big and small supercell, respectively, every 2 ps. This makes dose rates of 1.07 10^8 dpa/s and 1.37 10^8 dpa/s, respectively, by far higher than any experiments.
Indeed, any long-range (thermal) diffusion is hindered for any defects in our FPA simulations. Hence, our simulations likely describe low temperature cases where kinetics effects can be neglected. In addition, they can describe cases where migration of defects is impeded by some external factors like trapping at impurities, for example vacancies in Fe-C or interstitials loops for Fe-Cr [44, 45]. However, local recombination of Frenkel pairs and reorganization of defects still operate within few picoseconds [46, 47] and provide an annealing rate that counteracts the (high) dose rate of defects produced by FPA. In addition, dislocations can absorb defects in the entire supercell since capture radii are of the same order of magnitude as the size of the supercell, being 1 nm and 4 nm, respectively for vacancies and interstitials [48, 49].

In the second set of simulations, we explore the stability and the role of C15 clusters observed in FPA simulations. To do so, we partly follow recent works done by Monasterio *et al* [41] for investigating the swelling induced by SIAs clusters in iron. We introduce single interstitials one after the other (up to 500 interstitials) with a time interval of 1 ps, in the vicinity of preexistent C15 clusters. We consider two sizes of C15 clusters, each of them embedded in supercells of 96.86 Å of thickness with a square base of 177.67 × 178.88 $Å^2$. One C15 cluster contains 87 SIAs, and lies far above the stability limit of C15 cluster with respect to ½<111> loops [6], and close but slightly below the stability limit with <100> loops. The other C15 cluster is made of 49 SIAs, and is situated slightly below the stability limit given by the ½ <111> loops.

We perform the analysis of our simulations using Ovito [50]. Dislocations are determined using the DXA algorithm [51] using default parameters. Densities of ½<111> and <100> dislocations are then evaluated by dividing their total length by the total volume of the supercell. In addition, knowing that C15 atoms exhibit icosahedral coordination, we use the polyhedral template matching method [52]

to identify them. Once selected, we classify C15 clusters as a function of their size, starting from 12 C15 atoms, the smaller C15 cluster.

As explained extensively elsewhere [6, 15, 14], C15 clusters exhibit complex geometry which calls for specific notations and clarifications that we recall hereafter. The building block of C15 cluster corresponds to a Z16 Frank-Kasper polyhedron having 12 atoms at interstitial positions together with 10 vacancies around a specified bcc atomic site. Larger C15 clusters gather a set of Z16 Frank-Kasper polyhedron having centers situated on one, among four, diamond network, which underlies the initial bcc structure. The C15 size refers to the atoms of the C15 cluster that are in interstitial positions as well as the centers of the Z16 polyhedra. The C15 Laves phase is obtained from the bcc phase by replacing 2n bcc atoms with 3n C15 atoms. This gives, in the infinite C15 cluster, a factor two between the overall interstitials contained in the cluster and the atoms in interstitials positions. However, in our analysis, beyond the atoms in the interstitial positions we count also the centers of Z16 polyhedra giving what will be reported in the following as the C15 size. The rough factor, in the infinite size limit, between the overall SIAs number of C15 cluster and the total number of counted atoms in C15 cluster is 3.
In the following, C15 SIA clusters are denoted I_n^{C15} cluster, where n is the net number of SIAs, i.e., the number of additional atoms in the bcc lattice. For example, the smaller C15 cluster containing 12 C15 atoms (without the atom located in the center of the C15 cluster that shares a site from the bcc structure), has a net number of 2 SIAs (= 12 interstitials – 10 vacancies) and is denoted I_2^{C15} cluster.

III Results: Nucleation and transformation of C15 clusters

We start with the analysis of the first set of simulations where we apply the FPA methodology. We report evolutions of dislocation densities and C15 sizes with dose (dpa) on Figure 1 and on Figure 2, respectively, for small and big supercells. We note that evolutions of densities of dislocations as well as number and size of C15 clusters behave identically with dose for both sizes of supercell. In addition, evolution of microstructures look very similar too, as illustrated on snapshots at different doses in Figure 3 and in Figure 4. This means that using a moderate size of supercell around one million atoms is sufficient to capture most meaningful information.

In both simulations, with big and small supercells, different stages emerge. We observe that the nucleation of C15 clusters – bigger than I_2^{C15} cluster – occurs first, and before any dislocation (Figure 1 and Figure 2). Then, their size (y axis) and their number (color scaling) increase gently with irradiation dose.

At 0.01 dpa, ½<111> loops start to nucleate (see Figure 3 and Figure 4). Many of these loops are bound to an immobile C15 cluster (see Figure 3 and 4 at 0.02 dpa) conforming to observations done by Dérès *et al* [53]. At the same dose of 0.01 dpa, C15 clusters reach sizes of 40 C15 atoms or equivalently I_{11}^{C15} cluster. This size of cluster is much lower than the crossover between formation energies of ½<111> loops and C15 clusters. Nucleation of ½<111> loops from C15 clusters takes therefore a kinetic path rather than a thermodynamic one. Next, <100> loops come out for doses of around 0.02 dpa, with much lower density compared to ½<111> loops.

Subsequently, densities of both types of dislocations increase with irradiation dose. They show maxima at different values of dose, being around 0.1 dpa for ½<111> loops with densities of 4 10^{16} m^{-2} and between 0.2 and 0.4 dpa for <100> loops with densities of roughly 10^{16} m^{-2}. In between, we observe that the number of C15 clusters shows its maximum at 0.03-0.04 dpa with sizes smaller than I_{11}^{C15} cluster. This number decreases while the density of ½<111> loops increases, likely because the former feeds the latter as we will see in the following.

In parallel, sizes of some C15 clusters continue to increase with dose, even far above maxima of dislocations densities i.e. at above 0.4 dpa. Besides, loops interact to each other (at around 0.1 dpa and further) and progressively transform into forest of dislocations as can be seen on Figure 3 and on Figure 4. Some interactions belong to reactions suggested by Masters and Xu *et al* [16, 22] and mentioned in introduction. These reactions yield to nucleation of <100> loops or to larger ½<111> loops.

Densities of both ½ <111> and <100> dislocations decrease and reach steady state above 0.8 dpa, with density of dislocation of ½ <111> loops representing 90 % of the total, which is slightly more than seen by Peng *et al* [27] of around 80%. This value is in line with some experiments (see Chen *et al* [54] or Schäublin *et al* [44]) where a low amount of <100> loops is seen in irradiated iron below 300°C. Yet, comparisons remain not always relevant since the absolute ratio between 1/2<111> and <100> loops seen experiments can be biased by surfaces that readily eliminate 1/2<111> loops. Total density of dislocations stabilize at roughly 10^{16} m^{-2}, around two orders of magnitude higher than experimental observations at room temperature [55], but only 4 times higher than values obtained at 93K [44]. Combination of very high dose rates and temperature employed in our FPA simulations are certainly responsible for such overestimation, and it remains uneasy to rescale with temperature or dose rate [44, 56]. In addition, some C15 clusters of more than 153 C15 atoms survive, which corresponds to I_{51}^{C15} according to large-scale rules [6]. Few of them even reach sizes of more than 255

C15 atoms (or equivalently I_{85}^{C15} cluster size). At steady state, one observes a balance between creation of dislocations from C15 clusters and their formation.

We now turn to the second set of simulations in which are investigated the responses of I_{49}^{C15} and I_{87}^{C15} clusters to injection of interstitials in their vicinity. As we describe below, responses are strikingly different in term of C15 evolution as well as concerning the nature of dislocations that nucleate.

We consider first the behavior of the smaller C15 cluster, i.e. the I_{49}^{C15} cluster (147 C15 atoms), reported on Figure 5. Under the injection of interstitials, the I_{49}^{C15} cluster increases first its size by trapping small mobile interstitials induced by irradiation, as already put in light by Zhang *et al* [30]. The growth continues up to roughly I_{53}^{C15} cluster (159 C15 atoms) at which a ½<111> loop nucleates (snapshots on Figure 6). While ½<111> loop develops, the C15 size drastically decreases, feeding its growth with the contribution of injected interstitials. Injection of interstitials stops at 500 ps (500 interstitials injected one after the other every 1 ps). Subsequently, the entire system smoothly evolves toward a steady state. Density of dislocation stabilizes at around 750 ps, namely 250 ps after the end of interstitials injection. In parallel, primary cluster stabilizes at roughly I_{23}^{C15} (69 C15 atoms) leaving also around some C15 clusters smaller than I_{7}^{C15} (21 C15 atoms). This is expected since, for the M07 potential, I_{23}^{C15} is situated at the limit of the cross point of C15 cluster stability (between I_{20}^{C15} and I_{30}^{C15} with 20-90 C15 atoms) with respect to ½<111> loops [6].

The picture is quite different concerning the evolution of I_{87}^{C15} cluster (261 C15 atoms), as can be seen on Figure 7. The cluster decreases in size and a <100> loop nucleates (snapshots on Figure 8) at around I_{53}^{C15} (159 C15 atoms). The <100> loop develops and reaches a steady state at around 100 ps after the interruption of the injection of interstitials. In between and 150 ps after the nucleation of <100>, a ½<111> loop nucleates too. In turn, this ½<111> loop develops by steps and then reaches a steady state lately, around 500 ps after the end of injection. Its density gets similar to the <100> loop. Meanwhile, primary cluster stabilizes – at a lower size than previously – at around I_{13}^{C15} (39 C15 atoms) and comparable residues are left around in the form of clusters smaller than I_{7}^{C15} (21 C15 atoms).

Interestingly, both small and big C15 clusters contribute to the creation of loops at different degrees. While ½<111> loops come up from both cluster sizes, only the bigger one can help the nucleation of <100> loops. Therefore, their formation probability is obviously low since not all clusters can attain the required size. Nevertheless, FPA simulations show that some of them can reach large sizes dynamically, without their transformation into any loops.

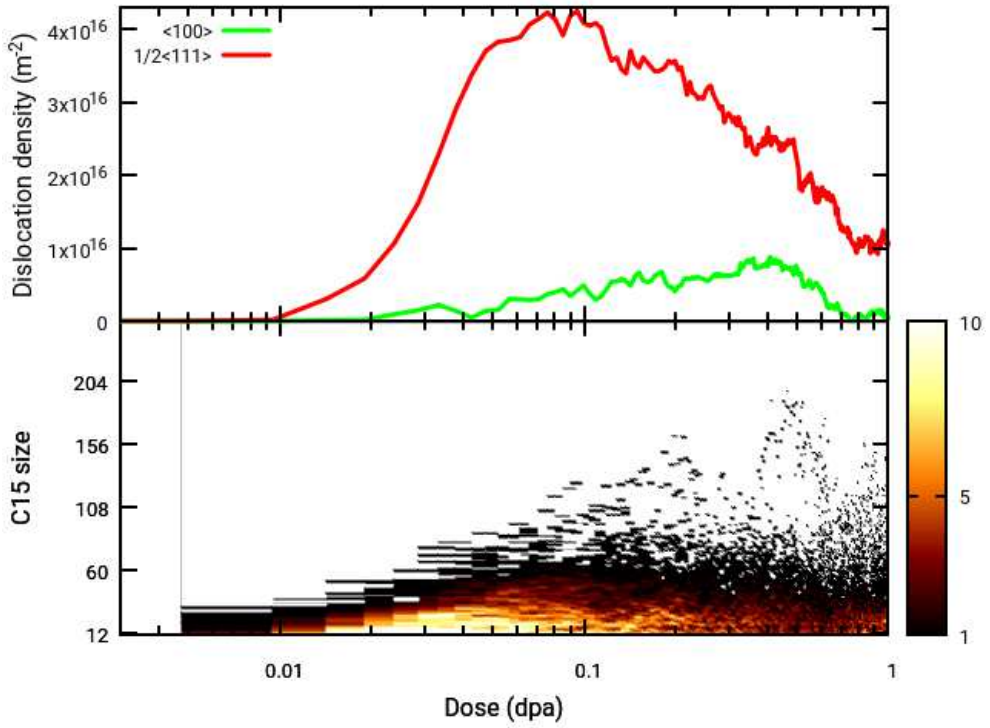

Figure 1 (color online): Upper panel shows the evolution of dislocation ½<111> and <100> loops density (at 300K), represented respectively by red and green lines and calculated by dividing their total length by the total volume of the supercell of 1458000 atoms. Lower panel shows C15 size as a function of dose in simulation supercell. In the lower panel is plotted the number of C15 clusters (color scaling) for each given C15 size.

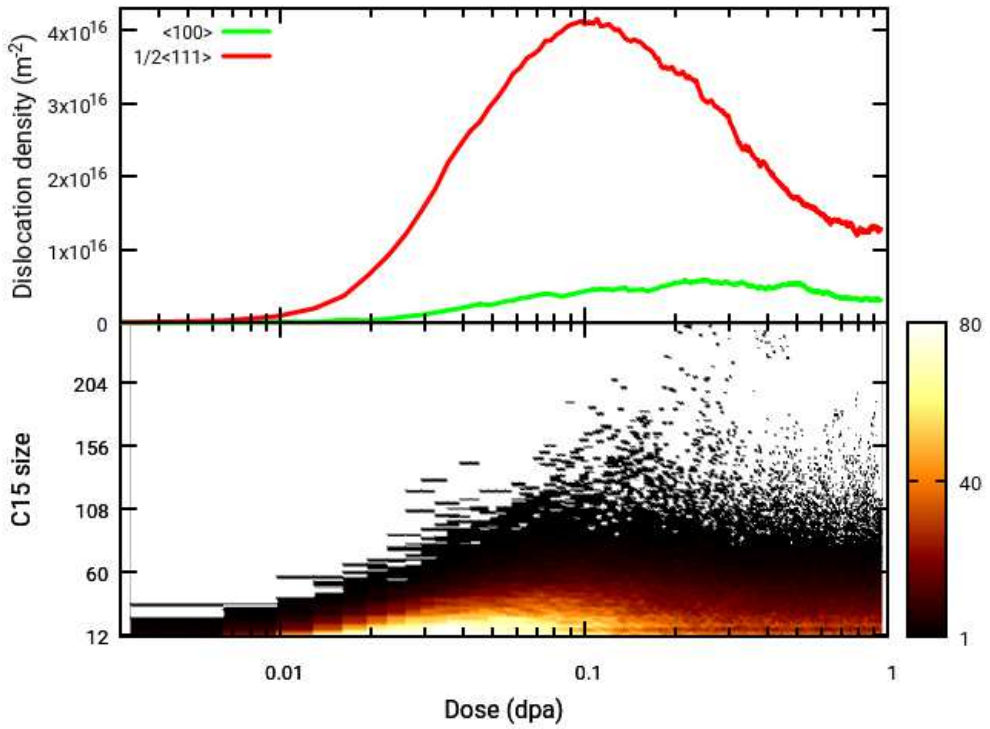

Figure 2 (color online): Evolution of dislocation ½<111> and <100> loops density, in the upper panel and C15 size in the lower panel as a function of dose in a simulation supercell containing 11664000 atoms (eight times bigger than the one of Figure 1) at 300K. Colors and legends are the same as in Figure 1 except the color scaling of the lower panel that has been rescaled by eight for comparison.

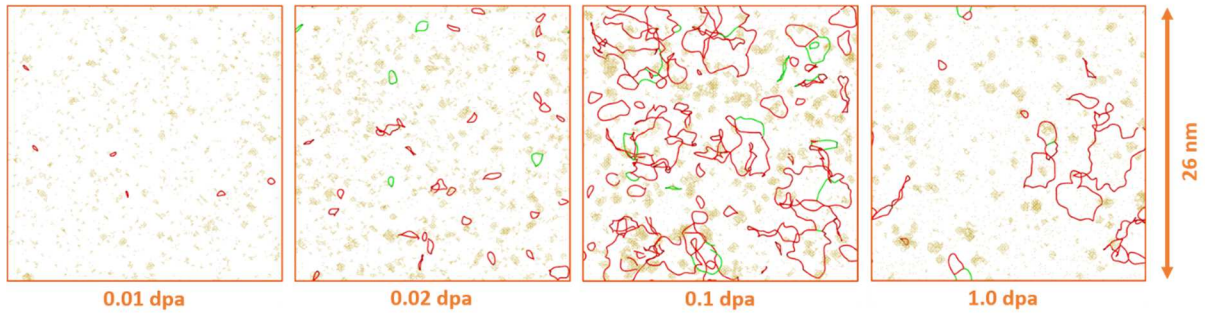

Figure 3. (color online) Selected snapshots of the evolution of dislocations and C15 clusters in iron as a function of doses for the small supercell (containing 1458000 atoms). Red and green lines represent respectively ½<111> and <100> loops. Yellow balls and sticks are for C15 atoms.

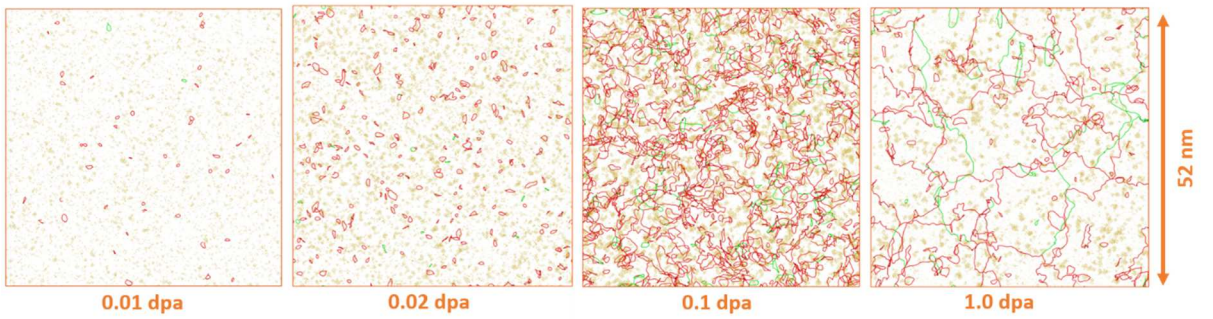

Figure 4: (color online) Selected snapshots of the evolution of dislocations and C15 clusters in iron as a function of doses for the big supercell (containing 11664000 atoms). Legends are the same as in Figure 3.

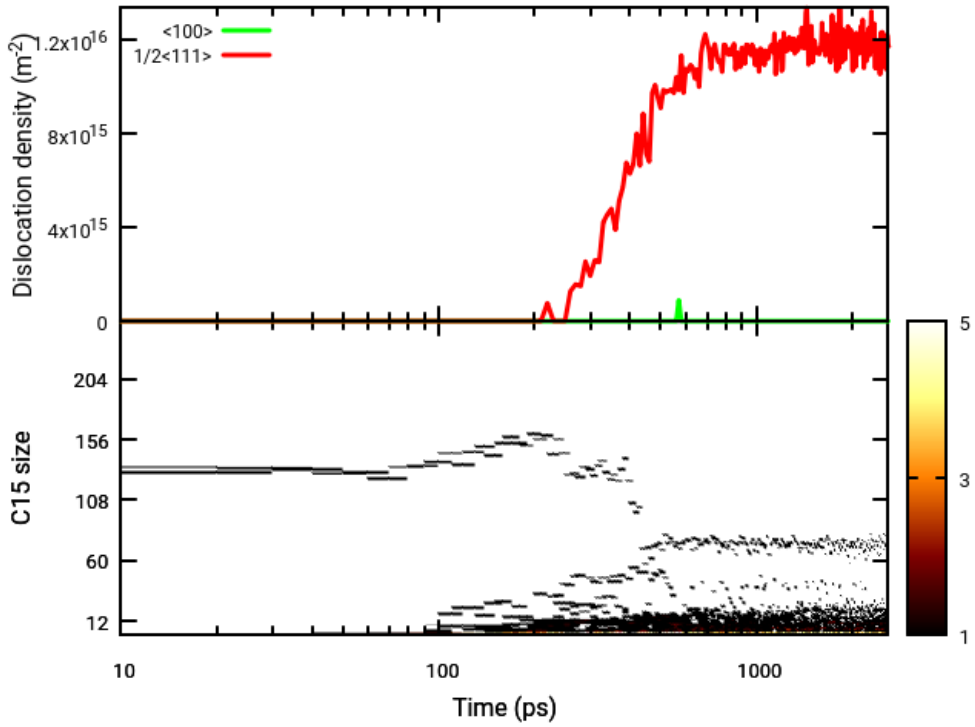

Figure 5: (color online) Evolution of dislocation density and C15 size as a function of time starting from a 49 SIA C15 cluster. 500 interstitials are injected, one after the other every 1 ps.

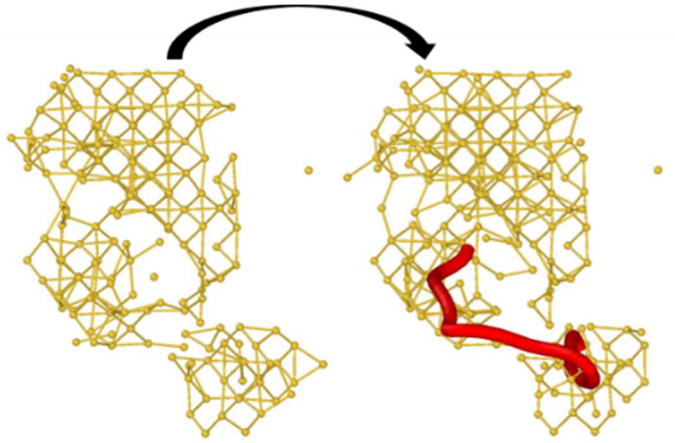

Figure 6: (color online) Nucleation of ½<111> dislocation from a 49 SIA C15 cluster. Legends are the same as in Figure 3.

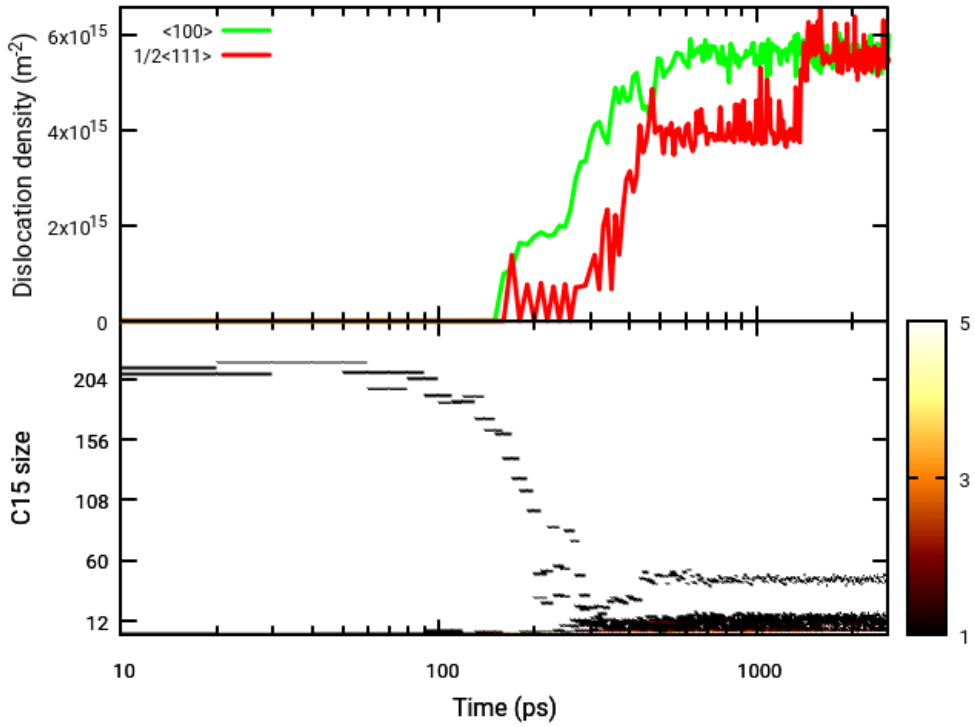

Figure 7: (color online) Evolution of dislocation density and C15 size as a function of time starting from an 87 SIA C15 cluster. 500 interstitials are injected, one after the other every 1 ps.

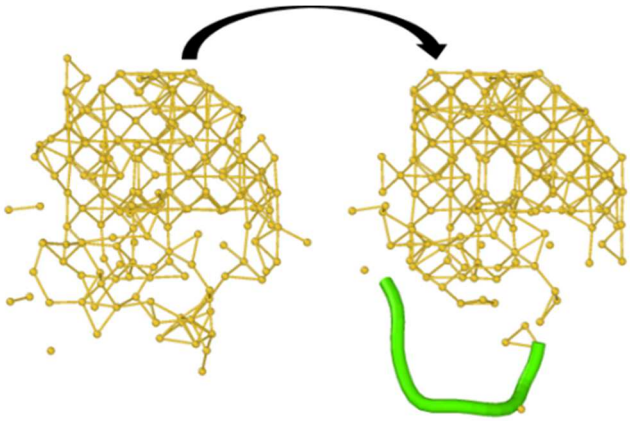

Figure 8: (color online) Nucleation of <100> loop from an 87 SIA C15 cluster. Legends are the same as in Figure 3.

IV Discussion: <100> loops nucleate from C15 clusters and ½ <111> loops

Our simulations suggest that the response of iron to irradiations can be decomposed into different stages. We have identified the following ones: (i) production of point defects by irradiation; (ii) their transformation into C15 clusters; then (iii) nucleation of ½ <111> loops (from C15 clusters) and; subsequently (iv) of <100> loops (from C15 clusters and ½<111> loops); finally (v) stabilization of a steady state in which all types of defects are present. Besides this sequence itself, some new features and mechanisms arise and may allow updating current knowledge on defects induced by irradiations in iron.

One of interesting results is the fact that nucleation of C15 clusters directly occurs from the accumulation of single SIAs. This result brings further support to previous observations that C15 clusters may (i) form in high-energy cascades as seen by Gao *et al* [31], Marinica *et al* [14] and Zarkadoula *et al*. [32] or (ii) appear as the result of overlap of cascades as shown by Byggmästar *et al.* [33]. While not surprising according to the general picture based on formation energies [14, 6], the assertion that C15 clusters dynamically nucleates from primary defects in irradiated iron is therefore significantly strengthened. Additionally, since our simulations reproduce electron irradiation at low temperature, as claimed by other authors [35, 36, 37], we provide an additional regime – SIAs transformation into C15 clusters under electron irradiation – to the ballistic one found by Byggmästar *et al* [33].
Another interesting result of our simulations is the fact that C15 clusters precede the formation of – *any* – loops, being ½ <111> or <100> ones. This is different from the results proposed by Byggmästar *et al* [33] who showed that ½ <111> loops form directly inside cascades, and before any C15 clusters. Nevertheless, present work feeds the work hypothesis done by Zhang *et al* [30] that C15 clusters exist prior to loops.
In addition, and besides the growth of C15 clusters itself which operates by capturing mobile interstitials as described by Zhang *et al* [30], their subsequent transformation – or not – into both ½ <111> and <100> loops is very informative. One observes that C15 clusters may readily transform into ½<111> loops when their size is above their stability limit. Wang *et al* [57] observed recently such a transformation with particular temperature / point defects conditions. These C15 clusters may also continue to grow and reach sizes that lead them to relax into <100> loops. Possibly, they may even further enhance their size, still fed by mobile interstitials produced by irradiation.
Yet, C15 clusters appear as one of the seeds for the nucleation of loops and especially the <100> loops in iron under irradiation. This is further supported by the fact that most dislocations begin and end into C15 clusters.
Indeed, the role of C15 clusters does not preclude any other well-known mechanism for the creation of <100> loops. Rather, we do see in our FPA simulations that complex self-interactions between ½<111> loops result in their formation as suggested by Masters [16] decades ago. While it is uneasy to decide if these interactions involve three ½<111> loops as pointed by Wang *et al* [24] recently, the formation of <100> loops likely requires two as explained by Marian *et al* [21] and by Xu *et al* [22].

Apart from these new features and mechanisms themselves, our results provide extra situations that promote nucleation of C15 clusters and of <100> loops from them. Recalling, our FPA simulations

operate at high dose rates. It reasonably corresponds to electron irradiation at low temperature [35, 36, 37]. No long-range diffusion is therefore allowed, but this does not impede short-range movements. Indeed, Frenkel pairs recombination [46, 47] as well as absorption of defects by dislocations [48, 49] act. Both ensure the entire transformations observed and therefore, short-range interactions alone explain the nucleation of C15 clusters and their transformation into loops and in particular <100> loops in irradiated iron.

V Conclusion

In the present work, we intensively use molecular dynamics simulations to investigate the response of iron to irradiation. For this purpose, we used the Frenkel pairs accumulation framework whose main characteristic is an accelerated introduction of damages. With these simulations, we expect to mimic reliably electron irradiation of iron at low temperature, knowing that thermal – i.e. long-range – diffusion is overlooked.

In such conditions, we find a complex interplay between the two main families of interstitial defects in bcc iron, the 2D defects – namely ½<111> and <100> loops – and the 3D ones –, i.e. C15 clusters. The present investigation reveals that: (i) C15 clusters appear in the very early stage of the microstructure evolution of irradiated iron, and prior to – *any* – loops and (ii) both ½<111> and <100> loops can directly nucleate from C15 clusters. Interestingly, some other well-known mechanisms – like the interactions between ½<111> loops – still operate for the transformation of ½<111> loops into <100>. Hence, the present study does not exclude any previous proposed mechanisms.

In addition, having proved that both C15 clusters and ½ <111> loops may yield <100> loops, we also establish that each mechanism envisioned previously as contradictory may rather collaborate. Further, C15 clusters may feed loops when thermal diffusion is hindered, while loops self-interactions may take over otherwise. This might explain the formation of <100> loops in dense systems as Fe-Cr [44], in which the diffusion of loops being blocked by the Cr, the formation of loops might happen via C15 clusters. In order to propose a hierarchy among these mechanisms more involved studies giving accurate statistics are needed.

Obviously, the effect of temperature and long-range diffusion are yet to be explored. In particular, one may wonder if high enough temperatures would modify the paths for the creation of C15 clusters and <100> loops as we describe above. Such a question could be addressed now, by implementing different mechanisms found herein in higher-level multi-scale simulations, like kinetic Monte-Carlo, cluster dynamics or mean-field approximation.

Acknowledgments

This work has been carried out within the framework of the EUROfusion Consortium and has received funding from the Euroatom research and training program 2014-2018 under grant agreement No 633053. The views and opinions expressed herein do not necessarily reflect those of the European Commission. The research leading to these results is partly funded by the European Atomic Energy Community's (Euratom) Seventh Framework Programme FP7/2007-2013 under grant agreement No. 604862 (MatISSE project)) and in the framework of the EERA (European Energy Research Alliance) Joint Programme on Nuclear Materials. The author(s) MCM acknowledge the support of the French Agence Nationale de la Recherche (ANR) under project project EPigRAPH ANR-14-CE07-0001.
MCM acknowledges support from the GENCI (CINES/CCRT/IDRIS) computer center under Grant A0050906973. MCM acknowledges François Willaime for encouraging C15 clusters studies. AC acknowledges Jean-Paul Crocombette for the fruitful discussions at the origin of the present work.

VI References

[1] Y. Matsukawa, and S.J. Zinkle, One-dimensional fast migration of vacancy clusters in metals, Science 318 (2007) 959.
[2] F. Willaime, C.-C. Fu, M.-C. Marinica, J. D. Torre, Stability and mobility of self-interstitials and small interstitials clusters in α-iron: ab-initio and empirical potential calculations, Nucl. Inst. Meth. Phys. B228 (2004) 92.
[3] D. Nguyen-Manh, A.P. Horsfield, and S.L. Dudarev, Self-interstitial defects in bcc transition metals: group specific trends, Phys. Rev. B73 (2006) R020101.
[4] D. A. Terentyev, T.P.C. Klaver, P. Olsson, M.-C. Marinica, F. Willaime, C. Domain, L Malerba, Self-Trapped Interstitial-Type Defects in Iron, Phys. Rev. Lett. 100 (2008) 145503.
[5] M.-C. Marinica, F. Willaime, N. Mousseau, Energy landscape of small clusters of self-interstitial dumbbells in iron, Phys. Rev. B83 (2011) 094119.
[6] R. Alexander, M.-C. Marinica, L. Proville, F. Willaime, K. Arakawa, M.R. Gilbert, and S.L. Dudarev, Phys. Rev. B94 (2016) 024103.
[7] P.-W. Ma, and S.L. Dudarev, Universality of point defect structure in body-centered cubic metals, Phys. Rev. Mater. 3 (2019) 013605.
[8] C. Domain, C. S. Becquart, Ab initio calculations of defects in Fe and dilute Fe-Cu alloys. Phys. Rev. B65 (2001) 024103.
[9] P. M. Derlet, D. Nguyen-Manh, S. L. Dudarev, Multiscale modeling of crowdion and vacancy defects in body-centered-cubic transition metals, Phys. Rev. B76 (2007) 054107.
[10] S. L. Dudarev, R. Bullough, P. M. Derlet, Effect of the alpha-gamma Phase Transition on the Stability of Dislocation Loops in bcc Iron, Phys. Rev. Lett. 100 (2008) 135503.
[11] C. C. Fu, F. Willaime, P. Odrejon, Stability and mobility of mono- and di-interstitials in α-Fe, Phys. Rev. Lett. 92 (2004) 175503.
[12] T. Amino, K. Arakawa, and H. Mori, Detection of one-dimensional migration of single self-interstitial atoms in tungsten using high-voltage electron microscopy, Sci. Rep. 6 (2016) 26099.
[13] C.-C. Fu, J. D. Torre, F. Willaime, J.-L. Bocquet, A. Barbu, Multiscale modelling of defect kinetics in irradiated iron, Nature Mater. 4 (2005) 68.
[14] M.-C. Marinica, F. Willaime, J.-P. Crocombette, Irradiation-Induced Formation of Nanocrystallites with C15 Laves Phase Structure in bcc Iron, Phys. Rev. Lett. 108 (2012) 025501.
[15] L. Dézerald, M.-C. Marinica, L. Ventelon, D. Rodney, and F. Willaime, Stability of self-interstitial clusters with C15 Laves phase structure in iron, J. Nucl. Mater. 449 (2014) 219.
[16] B. C. Masters, Dislocation Loops in Irradiated Iron, Nature 200 (1963) 254.
[17] P. Ehrhart, K. H. Robrock and H. R. Schober in Physics of Radiation Effects in Crystals edited by R.A. Johnson and A.N. Orlov (Elsevier, Amsterdam, 1986).
[18] B.L. Eyre, and R. Bullough, On the formation of interstitial loops in bcc metals, Phil. Mag. 12 (1965) 31.
[19] K. Arakawa, T. Amino, M. Isshiki, K. Mimura, M. Uchikoshi, and H. Mori, One-Dimensional Glide Motion of 'Naked' Nanoscale 1/2<111> Prismatic Dislocation Loops in Iron, ISIJ International 54 (2014) 2421.
[20] Y. N. Osetsky, A. Serra, and V. Priego, Interactions between mobile dislocation loops in Cu and α-Fe, J. Nucl. Mater. 276 (2000) 202.
[21] J. Marian, B. D. Wirth, J. M. Perlado, Mechanism of Formation and Growth of <100> Interstitial Loops in Ferritic Materials, Phys. Rev. Lett. 88 (2002) 255507.
[22] H. Xu, R. E. Stoller, Y. N. Osetsky, D. Terentyev, Solving the Puzzle of ⟨100⟩ Interstitial Loop Formation in bcc Iron, Phys. Rev. Lett. 110 (2013) 265503.

[23] K. Arakawa, T. Amino, and H. Mori, Direct observation of the coalescence process between nanoscale dislocation loops with different Burgers vectors, Acta Mater. 59 (2011) 141.
[24] X. Wang, N. Gao, Y. Wang, X. Wu, G. Shu, C. Li, Q. Li, B. Xu, and W. Liu, Formation of dislocation loop in bcc-Fe via the ternary loop reaction, Scripta Mater. 162 (2019) 204.
[25] J. Chen, N. Gao, P. Jung, T. Sauvage, A new mechanism of loop formation and transformation in bcc iron without dislocation reaction, J. Nucl. Mater. 441 (2013) 216.
[26] G.S. Khara, S.T. Murphy, and D. Duffy, Dislocation loop formation by swift heavy ion irradiation of metals, J. Phys.: Condens. Matter 29 (2017) 285303.
[27] Q. Peng, F. Meng, Y. Yang, C. Lu, H. Deng, L. Wang, S. De, and F. Gao, Shockwave generates <100> dislocation loops in bcc iron, Nature Comm. 9 (2018) 4880.
[28] A.F. Calder, D.J. Bacon, A.V. Barashev, and Y.N. Osetsky, Effect of mass of the primary knock-on atom on displacement cascade debris in α-iron, Phil. Mag. Lett. 88 (2008) 43.
[29] F. Granberg, J. Byggmästar, A.E. Sand, and K. Nordund, Cascade debris overlap mechanism of <100> dislocation loop formation in Fe and FeCr, Europhysics Letters 119 (2017) 56003.
[30] Y. Zhang, X.-M. Bai, M. R. Tonks, S. B. Biner, Formation of prismatic loops from C15 Laves phase interstitial clusters in body-centered cubic iron, Scripta Mater. 98 (2015) 5.
[31] F. Gao, D.J. Bacon, Y.N Osetsky, P.E.J. Flewitt, and T.A. Lewis, Properties and evolution of sessile interstitial clusters produced by displacement cascades in α-iron, J. Nucl. Mater. 276 (2000) 213.
[32] E. Zarkadoula, S.L. Daraszewicz, D.M. Duffy, M.A. Seaton, I.T. Todorov, K. Nordlund, M.T. Dove, and K. Trachenko, The nature of high-energy radiation damage in iron, J. Phys.: Condens. Matter 25 (2013) 125402.
[33] J. Byggmästar, F. Granberg, and K. Nordlund, Effects of short-range repulsive potential on cascade damage in iron, J. Nucl. Mater. 508 (2018) 530.
[34] Y. Limoge, A. Rahman, H. Hsieh, and S. Yip, Computer simulation studies of radiation induced amorphization, J. Non-Cryst. Solids 99 (1988) 75.
[35] M.J. Sabochick, and N.Q. Lam, Radiation-induced amorphization of ordered intermetallic compounds CuTi, $CuTi_2$, and Cu_4Ti_3: a molecular dynamics study, Phys. Rev. B43 (1991) 5243.
[36] T. Nagase, K. Takizawa, M. Wakeda, Y. Shibutani, and Y. Umakoshi, Electron-irradiation-induced solid-state amorphization caused by thermal relaxation of lattice defects, Intermetallics 18 (2010) 441.
[37] T. Nagase, K. Takizawa, and Y. Umakoshi, Electron-irradiation-induced solid-state amorphization in supersaturated Ni-Zr solid solutions, Intermetallics 19 (2011) 511.
[38] J.-P. Crocombette, A. Chartier, and W.J. Weber, Atomistic simulation of amorphization thermokinetics in lanthanum pyrozirconate, Appl. Phys. Lett. 88 (2006) 51912.
[39] A. Chartier, G. Catillon, and J.-P. Crocombette, Key role of the cation interstitial structure in the radiation resistance of pyrochlores, Phys. Rev. Lett. 102 (2009) 155503.
[40] A. Chartier, L. Van Brutzel, B. Pannier, and Ph. Baranek, Atomic scale mechanisms for the amorphisation of irradiated graphite, Carbon 91 (2015) 395.
[41] P.R. Monasterio, S. Yip, and B. Yildiz, Self-interstitial clusters in radiation damage accumulation: coupled molecular dynamics and metadynamics simulations, Eur. Phys. J. B86 (2013) 118.
[42] S. Plimpton, Fast parallel algorithms for short-range molecular dynamics, J. Comp. Phys. 117 (1995) 1.
[43] L. Malerba, M.-C. Marinica, N. Anento, C. Björkas, H. Nguyen, C. Domain, F. Djurabekova, P. Olsson, K. Nordlund, A. Serra, D. Terentyev, F. Willaime, and C.S. Becquart, Comparison of empirical interatomic potentials for iron applied to radiation damage studies, J. Nucl. Mater. 406 (2010) 19.
[44] R. Schäublin, B. Décamps, A. Prokhodtseva, and J.F. Löffler, On the origin of primary ½ a_0 <111> and a_0 <110> loops in irradiated Fe(Cr) alloys, Acta. Mater. 133 (2017) 427.

[45] T. Schuler, C. Barouh, M. Nastar, and C.-C. Fu, Equilibrium vacancy concentration driven by undetectable impurities, Phys. Rev. Lett. 115 (2015) 015501.
[46] P. Olsson, C.S. Becquart, and C. Domain, Ab initio threshold displacement energies in iron, Mater. Res. Lett. 4 (2016) 219.
[47] K. Nakashima, R.E. Stoller, and X. Xu, Recombination radius of a Frenkel pair and capture radius of a self-interstitial atom by vacancy clusters in bcc Fe, J. Phys.: Condens. Matter 27 (2015) 335401.
[48] V. Shastry, and T. Dias de la Rubia, The interaction between point defects and edge dislocations in BCC iron, J. Engineer. Mater. Tech. – Transactions of the ASME 121 (1999) 126.
[49] N. Anento, L. Malerba, and A. Serra, Edge dislocations as sinks for sub-nanometric radiation induced defects in α-iron, J. Nucl. Mater. 498 (2018) 341.
[50] A. Stukowski, Visualization and analysis of atomistic simulation data with OVITO – the Open Visualization Tool, Modelling Simul. Mater. Sci. Eng. 18 (2010) 015012.
[51] A. Stukowski, V.V. Bulatov, and A. Arsenlis, Automated identification of dislocations in crystal interfaces, Modelling Simul. Mater. Sci. Eng. 20 (2012) 085007.
[52] P. Mahler Larsen, S. Schmidt and J. Schiøtz, Robust structural identification via polyhedral template matching, Modelling Simul. Mater. Sci. Eng. 24 (2016) 055007.
[53] J. Dérès, L. Proville, M.-C. Marinica, Dislocation depinning from nano-sized irradiation defects in a bcc iron model, Acta Mater. 99 (2015) 99.
[54] J. Chen, F. Duval, P. Jung, R. Schäublin, N. Gao, and M.F. Barthe, Dislocation loops in ultra-high purity Fe(Cr) alloys after 7.2 MeV proton irradiation, J. Nucl. Mater. 503 (2018) 81.
[55] M. Hernández-Mayoral, Z. Yao, M.L. Jenkins, and M.A. Kirk, Heavy-ion irradiations of Fe and Fe-Cr model alloys Part 2: Damage evolution in thin-foils at higher doses, Phil. Mag. 88 (2008) 2881.
[56] A. Dunn, B. Muntfering, R. Dingreville, K. Hattar, and L. Capolungo, Displacement rate and temperature equivalence in stochastic cluster dynamics simulations of irradiated α-Fe, J. Nucl. Mater. 480 (2016) 129.
[57] H. Wang, N. Gao, G.-H. Lü, and Z.-W. Yao, Effects of temperature and point defects on the stability of C15 Laves phase in iron: a molecular dynamics investigation, Chin. Phys. B27 (2018) 066104.

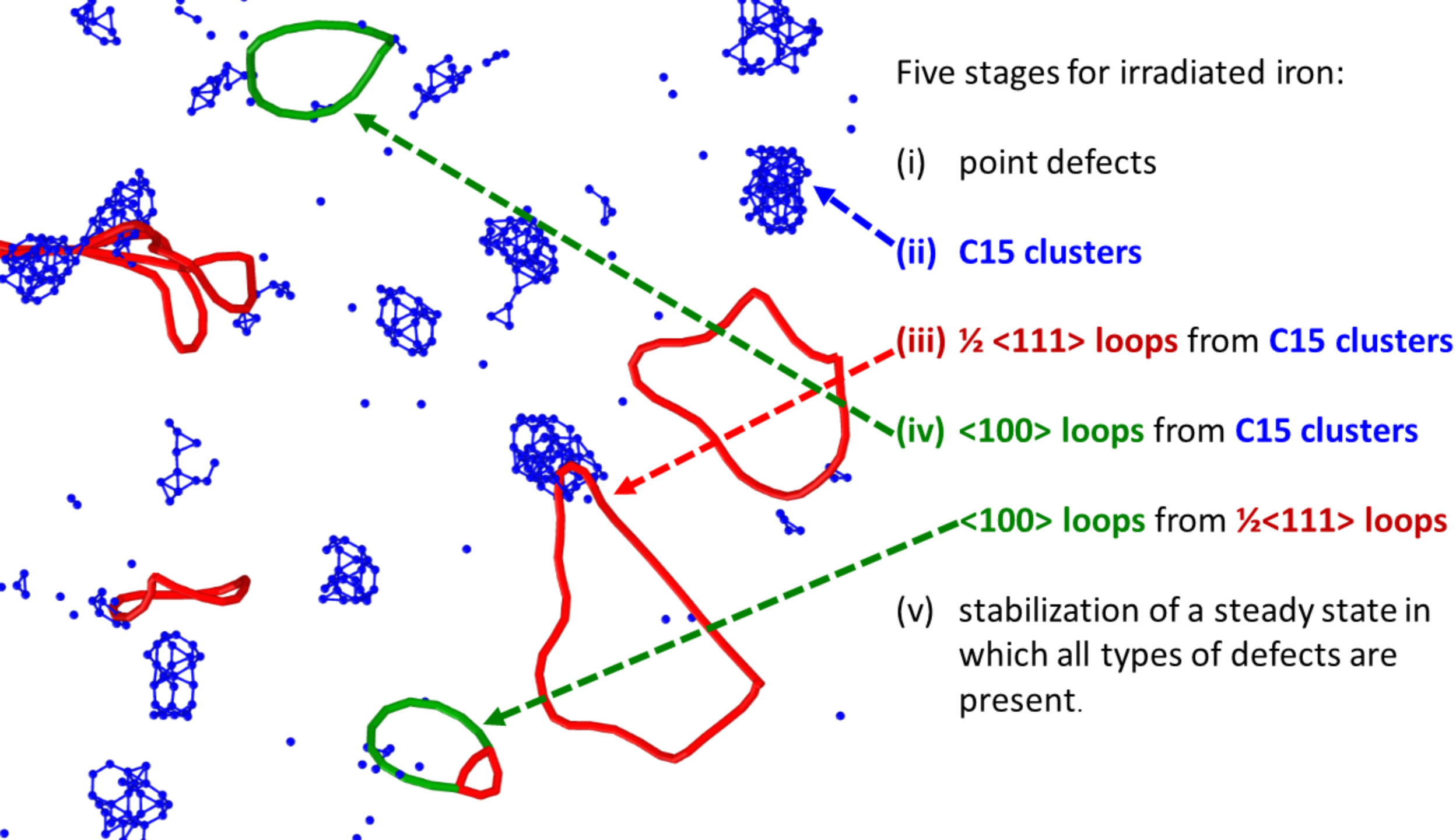

Five stages for irradiated iron:

(i) point defects

(ii) **C15 clusters**

(iii) **½ <111> loops** from **C15 clusters**

(iv) **<100> loops** from **C15 clusters**

<100> loops from **½<111> loops**

(v) stabilization of a steady state in which all types of defects are present.